



**HAL**  
open science

# Mapping Submerged Aquatic Vegetation along the Central Vietnamese Coast Using Multi-Source Remote Sensing

Tran Ngoc Khanh Ni, Hoang Cong Tin, Vo Trong Thach, Izuru Saizen, Cédric Jamet

► **To cite this version:**

Tran Ngoc Khanh Ni, Hoang Cong Tin, Vo Trong Thach, Izuru Saizen, Cédric Jamet. Mapping Submerged Aquatic Vegetation along the Central Vietnamese Coast Using Multi-Source Remote Sensing. ISPRS International Journal of Geo-Information, 2020, 9 (6), pp.395. 10.3390/ijgi9060395 . hal-04254893

**HAL Id: hal-04254893**

**<https://hal.science/hal-04254893>**



Submitted on 23 Oct 2023

**HAL** is a multi-disciplinary open access archive for the deposit and dissemination of scientific research documents, whether they are published or not. The documents may come from teaching and research institutions in France or abroad, or from public or private research centers.

L'archive ouverte pluridisciplinaire **HAL**, est destinée au dépôt et à la diffusion de documents scientifiques de niveau recherche, publiés ou non, émanant des établissements d'enseignement et de recherche français ou étrangers, des laboratoires publics ou privés.

Article

# Mapping Submerged Aquatic Vegetation along the Central Vietnamese Coast Using Multi-Source Remote Sensing

Tran Ngoc Khanh Ni <sup>1</sup>, Hoang Cong Tin <sup>1,\*</sup> , Vo Trong Thach <sup>2</sup>, Cédric Jamet <sup>3,4</sup>  and Izuru Saizen <sup>5</sup>

<sup>1</sup> Faculty of Environmental Science, University of Sciences, Hue University, Hue City 530000, Vietnam; tnkhanhni@husc.edu.vn

<sup>2</sup> Nhatrang Institute of Technology Research and Application, Nha Trang City 650000, Vietnam; votrongthach@nitra.vast.vn

<sup>3</sup> LOTUS, University of Science and Technology of Hanoi, Hanoi 100000, Vietnam; cedric.jamet@univ-littoral.fr

<sup>4</sup> CNRS, Université du Littoral Côte d'Opale, Université Lille, UMR 8187, LOG, Laboratoire d'Océanologie et de Géosciences, F 59000 Lille, France

<sup>5</sup> Graduate School of Global Environmental Studies, Kyoto University, Yoshida Honmachi, Sakyo-ku, Kyoto 606-8501, Japan; saizen.izuru.4n@kyoto-u.ac.jp

\* Correspondence: hoangcong tin@hueuni.edu.vn

Received: 7 May 2020; Accepted: 14 June 2020; Published: 16 June 2020



**Abstract:** Submerged aquatic vegetation (SAV) in the Khanh Hoa (Vietnam) coastal area plays an important role in coastal communities and the marine ecosystem. However, SAV distribution varies widely, in terms of depth and substrate types, making it difficult to monitor using in-situ measurement. Remote sensing can help address this issue. High spatial resolution satellites, with more bands and higher radiometric sensitivity, have been launched recently, including the Vietnamese Natural Resources, Environment, and Disaster Monitoring Satellite (VNREDSat-1) (V1) sensor from Vietnam, launched in 2013. The objective of the study described here was to establish SAV distribution maps for South-Central Vietnam, particularly in the Khanh Hoa coastal area, using Sentinel-2 (S2), Landsat-8, and V1 imagery, and then to assess any changes to SAV over the last ten years, using selected historical data. The satellite top-of-atmosphere signals were initially converted to radiance, and then corrected for atmospheric effects. This treated signal was then used to classify Khanh Hoa coastal water substrates, and these classifications were evaluated using 101 in-situ measurements, collected in 2017 and 2018. The results showed that the three satellites could provide high accuracy, with Kappa coefficients above 0.84, with V1 achieving over 0.87. Our results showed that, from 2008 to 2018, SAV acreage in Khanh Hoa was reduced by 74.2%, while gains in new areas compensated for less than half of these losses. This is the first study to show the potential for using V1 and S2 data to assess the distribution status of SAV in Vietnam, and its outcomes will contribute to the conservation of SAV beds, and to the sustainable exploitation of aquatic resources in the Khanh Hoa coastal area.

**Keywords:** Submerged aquatic vegetation; VNREDSat-1; Sentinel-2; Landsat-8; distribution map; temporal change map

## 1. Introduction

Vietnam is a coastal country located on the western side of the Eastern Sea (Biển Đông); it has 3260 km of coast, and a highly diverse assemblage of submerged aquatic vegetation (SAV) [1–3], which consists of two main groups—seagrasses and seaweeds. Seagrasses are flowering plants, while seaweeds are macro algae consisting of aggregating cells [2,4,5]. SAV is usually distributed in

coastal estuaries, brackish lagoons, and tidal regions, which are habitats and food sources for most aquatic organisms [4,5]. There are over 800 seaweed species in Vietnam, with about 121 of these having high economic value or potential to treat pollutants [2,6]. Fifteen seagrass species have been identified in Vietnamese coastal waters, and while the number of Vietnamese species is low, their root systems hold on to the ground, protecting benthic organisms and reducing coastal erosion. They also absorb carbon from the ocean, help purify the aquatic environment, and provide raw materials for several industries [2,6].

Khanh Hoa province is an important location in terms of the socio-economics and security defense of South-Central Vietnam; its shoreline extends from Dai Lanh commune to the end of Cam Ranh Bay, and features numerous estuaries, lagoons, and bays—and approximately 200 islands [7]. The coastal marine environment of Khanh Hoa is recognized as a high biodiversity area, with ecosystems containing an abundant and diverse flora and fauna [2,7]. The SAV of Khanh Hoa are considered to represent a high biodiversity hotspot in Vietnamese coastal waters.

It has been suggested that SAV in Khanh Hoa has been tending to decrease, both temporally and spatially, however, SAV dynamics have not been validated with any degree of accuracy. SAV ecosystems in Khanh Hoa province are widely distributed, in terms of their depths, substrates, and geographical locations, and include significant reserves [8–10]. These issues make them difficult to investigate and manage, suggesting that two modern tools—remote sensing and geographical information systems (GIS)—should be applied to overcome these challenges [11]. These tools can assess not only SAV distribution, but also its quantity and productivity, with high accuracy [12–14]. Numerous satellites that could be used to support managers in their planning for sustainable economic and social development exist, with many offering high spatial resolution, return rates, and numbers of bands [15–17].

Recently, scientists have used aerial photography, and satellite remote sensing techniques to examine SAV ecosystem characteristics and several of these studies have been published [18–28]. Setyawidati et al. (2006) assessed temporal changes to SAV in Chwaka Bay, Zanzibar (Tanzania), using Landsat satellite imagery over the period 1986–2003 without water deep correction [18], while Phinn et al. (2008) mapped seagrass distribution, ground coverage and biomass in Moreton Bay, Australia based on Hydrolight radiative-transfer model by three data sources, including Quickbird-2, Landsat-5 and Compact Airborne Spectrographic Imager type 2 (CASI-2) [19]. Noiraksar et al. (2014) applied depth invariant index (DII) and supervised classification method for ALOS AVNIR-2 (Advanced Land Observation Satellite-The Advanced Visible and Near Infrared Radiometer type 2) to determine the distribution of SAV in Sattahip marine area, Chon Buri province, Thailand [20]. Hoang et al. (2016) also used this method to map the distribution of SAV, surrounding Rottnest Island, Western Australia by WorldView-2 images [21]. Agnestesya et al. (2017) used WorldView-2, in this instance, Agnestesya et al. applied DII and principle component analysis using support vector machine classification to develop a distribution map for the SAV extant in the vicinity of Kotok and Bangkok islands, Indonesia [22].

In Vietnam, studies of marine species, substrate coverage, and biomass have helped build a database for each species and area [23–25]. In Khanh Hoa province, SAV ecosystems have been studied for some time; however, most of these studies have focused on the coastal area of Nha Trang, while studies on contiguous areas—such as Van Phong, Cam Ranh, Thuy Trieu or Nha Phu—remain limited [1,8]. Overall, there have generally been few studies in Vietnamese coastal areas where remote sensing and GIS techniques have been used to map SAV ecosystems, with Khanh Hoa being particularly neglected [1,9,10]. It is also noticeable that there have not been any studies using data from the first Vietnamese satellite—Vietnamese Natural Resources, Environment, and Disaster Monitoring Satellite (VNREDSat-1)—to map SAV ecosystem distribution in Vietnamese coastal waters. We noted as well that the majority of SAV mapping projects employed just one satellite data source [15,21,26,27], with few using two or more satellite data sources in their SAV status assessment [28]. Noting this, in the study reported here, the authors compared three different satellite data sets—as provided by Landsat-8, Sentinel-2, and VNREDSat-1—to map SAV ecosystems in the Khanh Hoa coastal area.

The objectives of the study reported here were therefore: (i) to evaluate the accuracy of three satellite remote sensing imagery sources for interpreting the distribution of SAV ecosystems; (ii) to define SAV ecosystem distribution in the Khanh Hoa coastal area; and (iii) to assess spatial and temporal changes to SAV ecosystems in the Khanh Hoa coastal area, thereby providing a baseline for improved monitoring of Khanh Hoa SAV, and to support their sustainable protection.

## 2. Materials and Methods

### 2.1. Study Area

The study area is located in South-Central Vietnam (Figure 1). Khanh Hoa province has the longest coastline in Vietnam, approximately 385 km from the edge of Dai Lanh commune to the South end of Cam Ranh Bay. The Khanh Hoa coast is diverse and complex, with a system of bays, islands, lagoons, and estuaries, and includes the continental shelf. Khanh Hoa has ~ 200 islands along its coast, and includes five lagoons and bays, including Van Phong Bay, Nha Trang Bay, Cam Ranh Bay, Nha Phu Lagoon, and Thuy Trieu Lagoon [7]. Of these locations, Van Phong Bay is in the North, while Cam Ranh Bay lies in the South, and has greater potential for use, as it is wider and deeper, with less sedimentation and fewer storms, than the former. Despite its name, Nha Phu Lagoon is not really a “lagoon”, like, say, Thuy Trieu Lagoon, being simply a small shallow bay, while Thuy Trieu Lagoon itself forms one of the 12 typical lagoons found along the central Vietnamese coast [7].

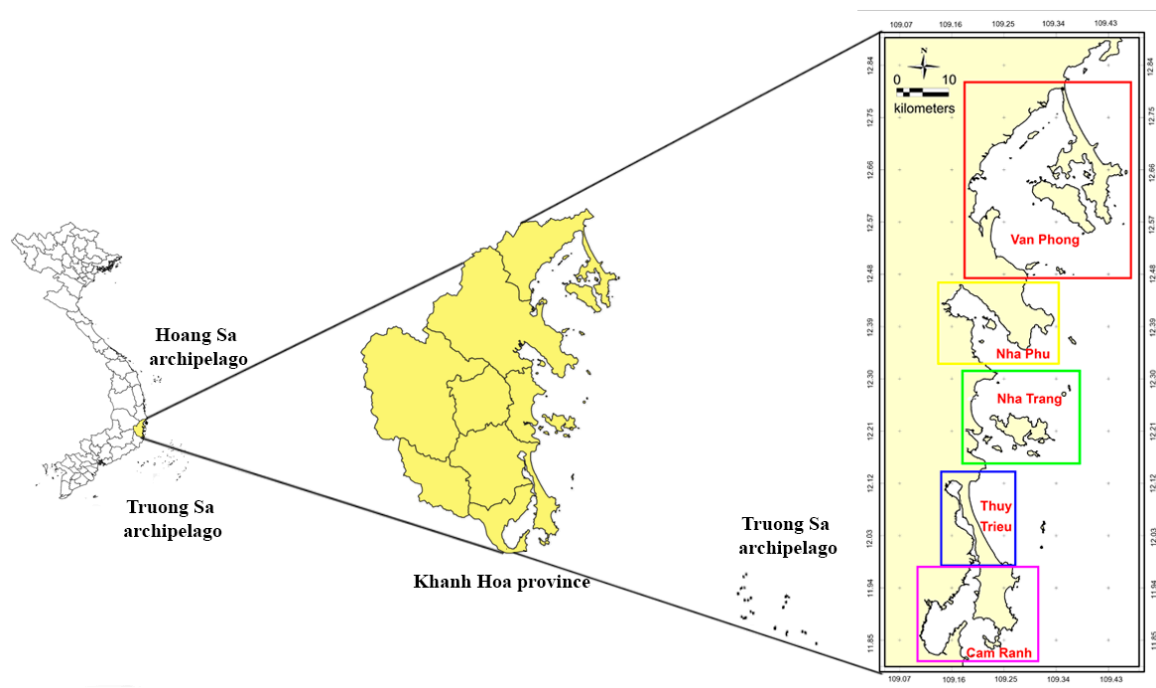


**Figure 1.** Study area with submerged aquatic vegetation (SAV) assessment sites.

The climate in Khanh Hoa province is dominated by the tropical monsoon climate and the nature of the ocean climate, so climate was relatively mild. There are two seasons in Khanh Hoa province: rainy and dry season [29]. The rainy season is short, from about mid-September to mid-December, rainfall often accounts for over 50% of the annual rainfall. From January to August are in the dry season, with an average of 2600 h of sunshine annually. The average annual temperature of Khanh Hoa is about 26.7 °C [29]. The relative humidity is about 80.5%. In the dry season, the early months from January to April are cool, the temperature is 17–25 °C. However, from May to August are hot, temperatures can reach 34 °C (in Nha Trang) and 37–38 °C (in Cam Ranh). In the rainy season, the temperature varies from 20–27 °C (in Nha Trang) and 20–26 °C (in Cam Ranh) [29].

## 2.2. Materials

### 2.2.1. Satellite Data

Data from three satellites were used to identify and monitor SAV distribution in the Khanh Hoa region: Landsat-8 (L8), Sentinel (S2), and VNREDSat-1 (V1). In Vietnam, remote sensing has been used since the 1960s, but the results have been limited by the absence of the technical support systems necessary to conduct research. Since the 2000s, more resources have become available, and more attention has been paid to remote sensing and GIS, which are now the focus of Vietnam's National Remote Sensing Center [1,8,25].

The L8 satellite includes two instruments—its Operational Land Imager (OLI) and Thermal Infrared Sensor (TIRS). The L8 has 12 bands with a 16-day repeat cycle. Radiometric resolution of L8 is 12-bit (16-bits when processed into Level-1 data products); Compared to previous Landsat satellites, L8 has new features and improved capabilities, such as the addition of two new spectral bands, one of which can be used to correct for atmospheric effects, while the other enables extraction of information from water masses, such as oceans, lakes, and rivers [30–32].

The S2 satellite includes a Multi-Spectral Instrument (MSI). Two S2s are currently in orbit—Sentinel-2A (S2A), which was launched on 23 June 2015, and Sentinel-2B (S2B), launched on 7 March 2017—with 180° phase separation between them. They have the same technical characteristics, including 13 bands in the visible and infrared spectra with a 10-day repeat cycle. Radiometric resolution is 12-bit. The signal to noise ratio of S2 is in the range 50–168. S2 satellites were the first optical Earth observation satellites to have three spectral bands located in the “red edge” band, providing important information about the state of plants, although these bands have not been commonly used, compared to the remaining bands. Data from L8 and the S2s have been applied to agriculture, geology, and land use–land change mapping, and to the assessment of air and water quality in various ecosystems, including lakes, rivers, and coastal ecosystems [33].

The Vietnamese Natural Resources, Environment, and Disaster Monitoring Satellite (VNREDSat-1) was the first Vietnamese satellite, launched on 7 May 2013, and including one instrument, the New AstroSat Optical Modular Instrument (NAOMI). NAOMI has fewer spectral bands than either L8 or S2, and includes four multi-spectral bands, each with a spatial resolution of 10 m (Table 1). V1 repeat cycle is more than L8 and S2, has a 29 days repeat cycle. Data from this satellite have been used for several environmental monitoring projects; the data are available from the end of 2013, and they has proven to be effective in several fields, although very few researchers have used them for coastal resources monitoring [34,35]. There has been one study on wetland ecosystems, carried out by Nguyen [36], while none concerning SAV distribution have been published. The wavelengths and spatial resolution characteristics of each sensor are listed in Table 1.

### 2.2.2. Data Collection

Maps and other documentation related to SAV studies, such as annual statistics, natural and socio-economic data, and reports on the status and planning of Khanh Hoa province, were collected from the Department of Natural Resources and Environment, People's Committee of Khanh Hoa province.

Multi-spectrum remote sensing data from V1, L8, and S2 were also acquired. L8 and S2 imagery were collected from the Glovis and EarthExplorer image databases (The United States Geological Survey (USGS), USA), while V1 data were supplied by the Vietnamese Centre for Control and Exploitation of Small Satellites. Landsat data have two images each year, and these were used to create the SAV distribution map for 2018, while S2 data, with three images, were used to create an SAV status map for 2019. The V1 data source has the highest number of images (nine images), and these were acquired for 2017. The remote sensing data sources used in this study have been summarized as Table 2.

**Table 1.** Wavelengths and spatial resolution characteristics of Landsat 8, Sentinel-2, and Vietnamese Natural Resources, Environment, and Disaster Monitoring Satellite (VNREDSat-1) sensors.

Spectrum	Landsat 8			Sentinel-2A			VNREDSat-1		
	Band	Center Wavelength ( $\mu\text{m}$ )	Spatial Resolution (m)	Band	Center Wavelength ( $\mu\text{m}$ )	Spatial Resolution (m)	Band	Center Wavelength ( $\mu\text{m}$ )	Spatial Resolution (m)
Coastal	B1	0.433	30	B1	0.443	60	-	-	-
Blue	B2	0.483	30	B2	0.490	10	B1	0.490	10
Green	B3	0.560	30	B3	0.560	10	B2	0.550	10
PAN	B8	0.640	15	-	-	-	-	-	-
Red	B4	0.660	-	B4	0.665	10	B3	0.660	10
Red edge 1	-	-	-	B5	0.705	20	-	-	-
Red edge 2	-	-	-	B6	0.740	20	-	-	-
Red edge 3	-	-	-	B7	0.783	20	-	-	-
NIR	B5	0.865	30	B8	0.840	10	B4	0.830	10
Red edge 4	-	-	-	B8a	0.865	20	-	-	-
Water aerosol	-	-	-	B9	0.945	60	-	-	-
SWIR-1	B6	1.650	30	B10	1.375	60	-	-	-
SWIR-2	B7	2.200	30	B11	1.610	20	-	-	-
SWIR-3	-	-	-	B12	2.190	20	-	-	-
Cirrus	B9	1.375	30	-	-	-	-	-	-

**Table 2.** Satellite image data used for SAV mapping and changes detection.

Year	Satellite Sensor	No	Image ID	Acquired Date	Time (GMT time)	Spatial Resolution (m)
2008	Landsat-5	1	LT05_L1TP_123051_20080717_20161030_01_T1	17/07/2008	02:47	30 × 30
		2	LT05_L1TP_123052_20080717_20161030_01_T1	17/07/2008	02:48	30 × 30
2015	VNREDSat-1	1	VNREDSAT_1_2015218_11982_3074_MS.lv0 _V20150806_031919X_1A	06/08/2015	03:19	10 × 10
		2	VNREDSAT_1_2015218_11982_3074_MS.lv0 _V20150814_032202X_1A	14/08/2015	03:22	10 × 10
2017	VNREDSat-1	3	VNREDSAT_1_2017191_22274_3076_MS.lv0 _V20170710_031455_X1A	10/07/2017	03:14	10 × 10
		4	VNREDSAT_1_2017191_22274_3076_MS.lv0 _V20170710_031457_X1A	10/07/2017	03:14	10 × 10
		5	VNREDSAT_1_2017191_22274_3076_MS.lv0 _V20170710_031500_X1A	10/07/2017	03:15	10 × 10
		6	VNREDSAT_1_2017191_22274_3076_MS.lv0 _V20170710_031502_X1A	10/07/2017	03:15	10 × 10
		7	VNREDSAT_1_2017191_22274_3076_MS.lv0 _V20170710_031505_X1A	10/07/2017	03:15	10 × 10
		8	VNREDSAT_1_2017191_22274_3076_MS.lv0 _V20170710_031507_X1A	10/07/2017	03:15	10 × 10
		9	VNREDSAT_1_2017191_22274_3076_MS.lv0 _V20170710_031510_X1A	10/07/2017	03:15	10 × 10
2018	Landsat-8	1	LC08_L1TP_123051_20180510_20180517_01_T1	10/05/2018	03:00	30 × 30
		2	LC08_L1TP_123052_20180510_20180517_01_T1	10/05/2018	03:00	30 × 30
2019	Sentinel-2A	1	L1C_T49PBP_A018805_20190128T031602	28/01/2019	06:07	10 × 10
		2	L1C_T49PCQ_A018805_20190128T031602	28/01/2019	06:07	10 × 10
		3	L1C_T49PCP_A018805_20190128T031602	28/01/2019	06:07	10 × 10

## 2.3. Methods

### 2.3.1. Field Surveys

Investigations were conducted from Van Phong Bay to Cam Ranh Bay, in two phases: phase 1 covered 18–22 June 2018, and phase 2 from 17–21 October 2018. Survey sites can be seen in Figure 2.

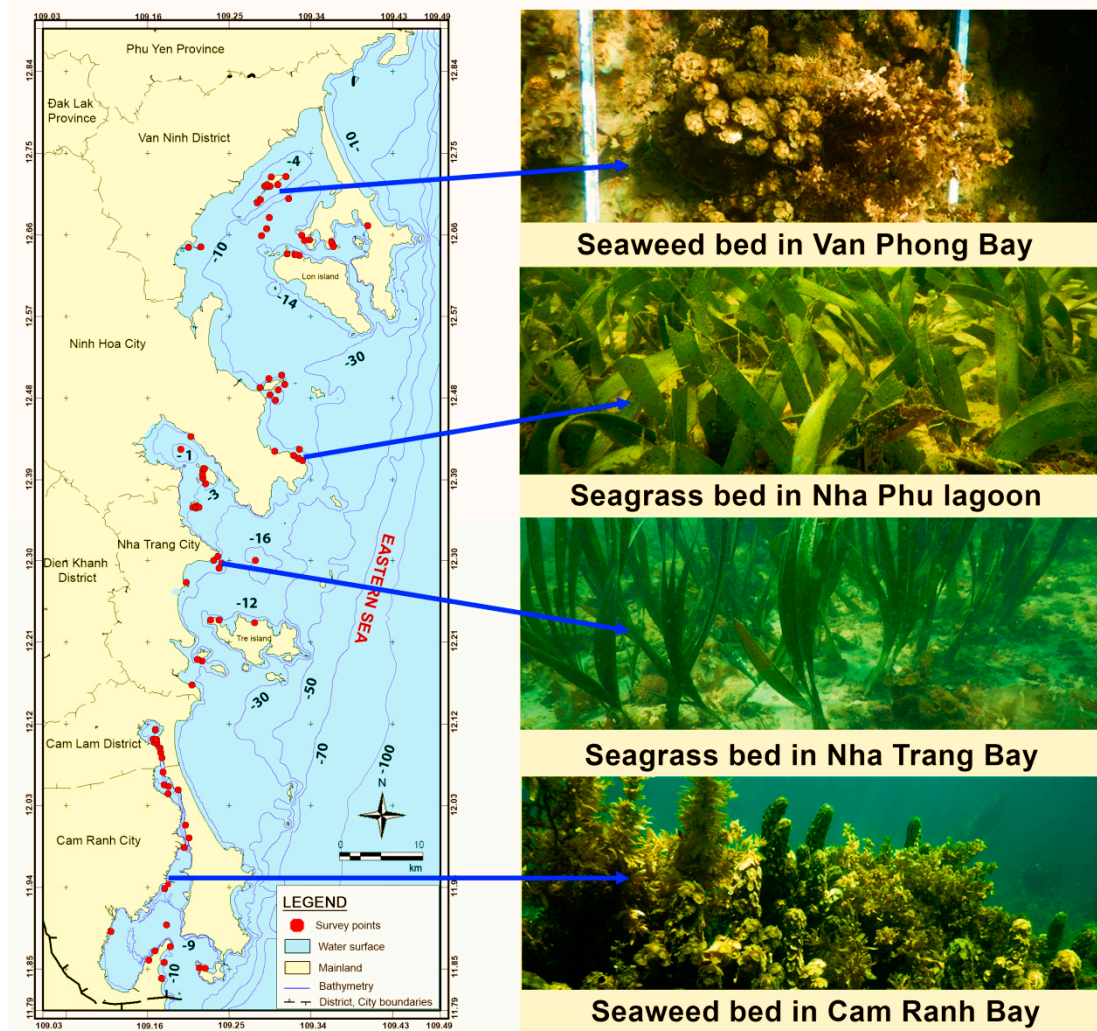






**Figure 2.** Survey sites along the Khanh Hoa coast, with pictures of various substrates (the blue lines in the ocean are isobaths).

SAV distribution at the study sites was observed using a motorboat and diving along transects in the direction from the shore seaward, until either water column depth reached 10 m, or SAV was no longer seen. Global Positioning System (GPS) positions were recorded for each survey point, and the substrate form and structure were also logged for each area. Substrates were classified as being either SAV, rock–coral, or sandy/mud bottom, as shown in Table 3. A total of 155 sample sites were established, including 18 deep water sites, 47 sandy sites, 54 SAV sites, 16 mud–sand sites, and 20 rock–coral sites. The positions of the 155 sample sites were located by GPS, and used as ground truthing points for later satellite image interpretation.

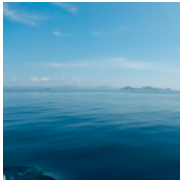


**Table 3.** Characteristics of ground truthing points in the Khanh Hoa coastal area.

Layers	Images	Locations	Characteristics
Deep water		Nha Trang Bay	The area was covered with water > 10 m deep
SAV		Van Phong Bay	Plants here grew completely underwater, including seagrass and seaweed
Sandy bottom		Bip island	Sandy bottom area. SAV species were not found on this bottom type, which was < 10 m deep
Mud–sandy bottom		Thuy Trieu lagoon	These areas have muddy or mixed mud and sand substrates. SAV species were not found on this bottom type, which was < 10 m deep
Rock–coral bottom		My Giang	The area included corals or rocks, and was < 10 m deep; SAV were found on this bottom type, with < 5% coverage

2.3.2. SAV Spatial Distribution and Area Change Mapping

Data collection, analysis, and processing were carried out using ENVI 5.5 and MapInfo 12.0 software. The process flow chart for mapping SAV temporal changes can be seen in Figure 3.

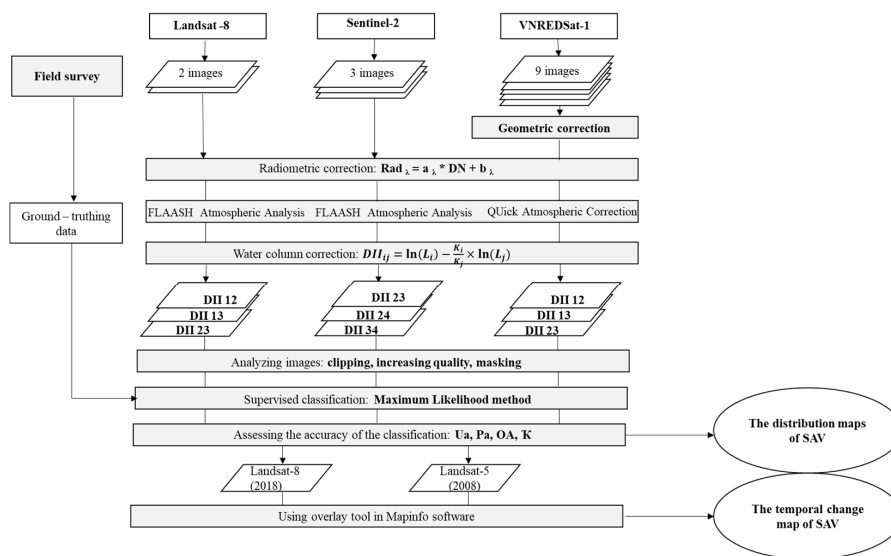


**Figure 3.** Process flow chart for establishing SAV distribution and temporal change mapping.

Geometric correction: this step was done after imagery had been obtained from suppliers, to register the satellite image coordinates [14,19]. In this study, the Universal Transverse Mercator (UTM)-The World Geodetic System 84 (WGS84)-Zone 48 projection system was used for the Landsat and S2 imagery, while the GEOGRAPHIC-WGS84 system was applied to V1 imagery. We therefore needed this step in order to unify the geographic coordinates of the imagery according to the UTM-WGS84-Zone 48 projection system. V1 imagery also contained geometric distortions, as received from the satellite, and so prior to atmospheric correction, it was corrected geometrically, to reduce the deviations encountered during photography, and to convert them into local geographic coordinates using other reference data sources (UTM project, WGS84 datum).

Radiometric correction: the purpose of this step was to convert the digital number of each image pixel into spectral radiation, using Equation (1) [37]:

$$\text{Rad}_\lambda = a_\lambda * \text{DN} + b_\lambda, \quad (1)$$

where  $\text{Rad}_\lambda$  represents Top of atmosphere (TOA) spectral radiance (as Watts/(m<sup>2</sup>\*srad\* $\mu\text{m}$ )), DN refers to the digital number of the band to be corrected,  $a_\lambda$  (gain value) stands for a band-specific, multiplicative rescaling factor from the image header, and  $b_\lambda$  (offset/bias value) represents a band-specific, additive rescaling factor from the image header. Gain and offset/bias values were provided in Landsat, S2 and V1 metadata files.

Atmospheric correction: the purpose of this step was to remove contributions from the atmosphere—which could include aerosols, dust, gas and air molecules [38]—to the total signal measured by the remote sensor, in order to obtain just that part of the signal referring to the sea. Use of atmosphere corrected image is to potentially improve the extraction of surface parameters and to produce more accurate surface reflectance. In this study, Landsat and S2 imagery were corrected using the Fast Line-of-sight Atmospheric Analysis of Hypercubes (FLAASH) method, in ENVI 5.5 [39]. For V1 imagery, the atmospheric impact was removed using the QUick Atmospheric Correction (QUAC) model because FLAASH method was no supporting V1 image.

The FLAASH model corrects the atmosphere for data in the visible through near-infrared and shortwave infrared ranges, up to 3  $\mu\text{m}$ , for super-spectral or multi-spectral imagery, calculating the atmospheric radiation transmission pattern using the most recent MODerate resolution atmospheric TRANsmission (MODTRAN) information [39].

The QUAC model is an atmosphere correction method for multi-spectral imagery applied through the shortwave infrared band (VNIR-SWIR). Unlike the FLAASH method, it determines atmospheric compensation parameters directly from information contained in the scene, without needing supporting information. QUAC performs a more accurate atmospheric correction than FLAASH, which usually produces spectral reflectance within approximately +/- 15%, based on physical methods [39].

Water column correction: the purpose of this step was to remove influencing factors stemming from dissolved or solid particles in the water column—including phytoplankton, colored dissolved organic matter (CDOM), and total suspended solids (TSS) [40]—which reduce light transmission from the surface to the euphotic depth. This step was based on calculating the depth invariant index (DII), which is the linear relationship (logarithm) between the surface reflectance spectrum of band i and band j, according to the randomly selected sandy bottom points at different depths. The principle of applying DII is that when light penetrates the water, its intensity decreases exponentially as the depth increases [41].

This index allowed conversion of surface reflectance and bottom reflection, and we had a total of 101 points, including 47 sandy points and 54 SAV points, from which to build the linear relationship between the reflection spectra of image band pairs. The linear relationship of band pairs, using randomly selected sand beds at different depths, formed the basis of the DII calculation, which was completed using Equation (2) [40]:

$$L_i = L_{si} + A_i * R_i * \exp(-K_i * f * Z) \quad (2)$$

This index was developed by Lyzenga in 1981; it does not require measuring the reflectance at the survey points but rather determines it through information directly on the image band. An improved formula was introduced by Lyzenga (2003), using a combination of multiple image bands, as shown in Equation (3) [40].

$$DII_{ij} = \ln(L_i) - \frac{K_i}{K_j} \times \ln(L_j), \quad (3)$$

where DII stands for the depth invariant index,  $L_i$  and  $L_j$  represent the outputs from atmospheric corrections for bands  $i$  and  $j$  respectively,  $K_i/K_j$  denotes the ratio of the water attenuation coefficients in bands  $i$  and  $j$ , and was calculated using Equation (4):

$$\frac{K_i}{K_j} = \frac{\sigma_{ii} - \sigma_{ij}}{2\sigma_{ij}} + \sqrt{\left(\frac{\sigma_{ii} - \sigma_{ij}}{2\sigma_{ij}}\right)^2 + \left(\frac{\sigma_{jj} - \sigma_{ij}}{2\sigma_{ij}}\right)^2} + 1, \quad (4)$$

in which  $\sigma_{ii}$  and  $\sigma_{jj}$  represent the variance of bands  $i$  and band  $j$  respectively, and  $\sigma_{ij}$  stands for the covariance of band  $i$  and band  $j$ .

We calculated  $K_i/K_j$  coefficients for the Landsat, V1, and S2 bands from the spectral reflection variance, and then selected the three band pairs with the best correlation. Table 4 shows the  $K_i/K_j$  ratios of the V1, L8, and S2 band pairs.

**Table 4.** Band pair  $K_i/K_j$  ratios.

$K_i/K_j$	VNREDSat-1	Landsat-8	Sentinel-2
$K_1K_2$	1.06517	1.13717	
$K_1K_3$	0.83167	1.47007	
$K_1K_4$	2.79363	1.46777	
$K_2K_3$	0.78698	1.28919	0.84158
$K_2K_4$	3.05801	1.27390	2.94201
$K_3K_4$	4.07538	0.97352	1.53698

Depth invariant indexes, estimated using the different  $K_i/K_j$  coefficients for V1, have been presented in Figure 4.

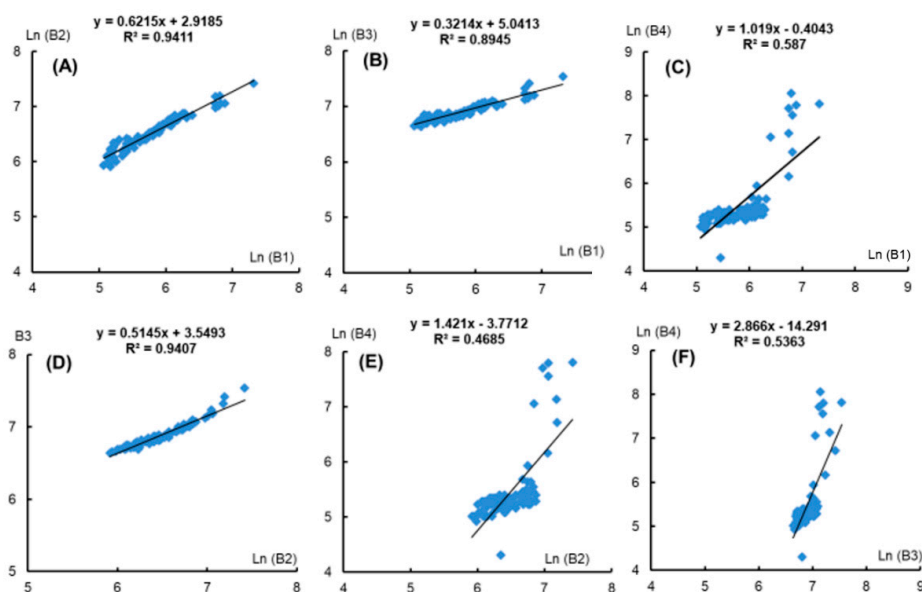


**Figure 4.** Several linear logarithm relationships of reflectance spectra between band  $i$  and band  $j$  from VNREDSat-1 imagery: (a) band 1 and band 2; (b) band 1 and band 3; (c) band 1 and band 4; (d) band 2 and band 4; band 3 and band 4.

$$\begin{aligned} \text{DII}_{12} &= \text{Ln} (B1) - 1.065169 * \text{Ln} (B2); R^2 = 0.941 \\ \text{DII}_{13} &= \text{Ln} (B1) - 0.831672 * \text{Ln} (B3); R^2 = 0.895 \\ \text{DII}_{14} &= \text{Ln} (B1) - 2.793626 * \text{Ln} (B4); R^2 = 0.587 \\ \text{DII}_{23} &= \text{Ln} (B2) - 0.786978 * \text{Ln} (B3); R^2 = 0.941 \\ \text{DII}_{24} &= \text{Ln} (B2) - 3.058009 * \text{Ln} (B4); R^2 = 0.469 \\ \text{DII}_{34} &= \text{Ln} (B3) - 4.075378 * \text{Ln} (B4); R^2 = 0.536 \end{aligned}$$

The correlation coefficients for the reflectance spectra of band 1 and 2, band 1 and 3, and band 2 and 3 were the highest, so we selected three new DII bands (DII<sub>12</sub>, DII<sub>13</sub>, DII<sub>23</sub>) for further classification. The same procedure was then applied to S2 and L8 data, and the correlation coefficients for each image channel have been listed in Table 5.

**Table 5.** Reflectance spectrum correlation coefficients for each band pair.

Bands	Reflectance Spectrum Correlation Coefficient (R <sup>2</sup> )		
	Landsat-8	Sentinel-2	VNREDSat-1
b1b2	0.925	-	0.941
b1b3	0.965	-	0.895
b1b4	0.855	-	0.587
b2b3	0.948	0.934	0.941
b2b4	0.918	0.561	0.469
b3b4	0.922	0.703	0.536

Analyzing and processing images: after water column correction, the remote sensing data were processed through further steps, such as clipping, increasing quality, and masking. Clipping allowed us to remove non-study areas covered by the imagery, focusing on just the main Khanh Hoa coast, while masking allowed us to hide land layers not involved in our work. These processing steps contributed to improving image quality in preparation for classification.

Supervised classification: the Maximum Likelihood method was used for classification, based on survey points for different bottom types [42]. This method allocates each pixel to the most probable class from the variance–covariance matrix, statistical indicators, and mean vector of each category, based on Bayes theorem. This resulted in creation of five classified layers, using Equation (5) [16,43].

$$P(X|Wi) = (2\pi)^{-0.5n} |S_i|^{-0.5} \exp[-0.5(X - \bar{X}_i)^T (S_i^{-1} (X - \bar{X}_i))], \quad (5)$$

This probability density function applies (x) as an arbitrary pixel, (Wi) as class (i), and (S) as the variance–covariance matrix of class (i), derived from training samples, and characterized as the basic function in the Maximum Likelihood Classification algorithm by assuming that the values in each spectral band were normally distributed. The five classes were characterized in Table 3.

Assessing the accuracy of the classification: the accuracy of the classification was based on a standard confusion matrix. Accuracy was checked using four coefficients, User accuracy (Ua), Producer's accuracy (Pa), Overall Accuracy (OA), and the Kappa coefficient (K). Kappa coefficients range from 0 to 1, and a desired value is usually > 0.7 [44,45]. Ua occurs when pixels separating a single class are allocated into other classes, while Pa is the ratio of the pixels in a column (the total pixels not correctly classified for each class in the reference data) and the total pixels in the column (the total pixels for that class in the reference data). OA is the ratio between the total number of correct pixels and the total number of pixels in the confusion matrix—which is shown in Table 6 [44,45].

**Table 6.** Confusion matrix table for calculating Overall, User, and Producer accuracies.

Object Classes	Class 1	Class 2	Class 3	Total ( $x_{i+}$ )	User accuracy (%)
Class 1	$x_{11}$	$x_{12}$	$x_{13}$	$x_{1+}$	$= (x_{11}/x_{1+}) * 100$
Class 2	$x_{21}$	$x_{22}$	$x_{23}$	$x_{2+}$	$= (x_{22}/x_{2+}) * 100$
Class k	$x_{31}$	$x_{32}$	$x_{33}$	$x_{3+}$	$= (x_{33}/x_{3+}) * 100$
Total ( $x_{+i}$ )	$x_{+1}$	$x_{+2}$	$x_{+3}$	$N = x_{1+} + x_{2+} + x_{3+}$	
Producer accuracy (%)	$= (x_{11}/x_{+1}) * 100$	$= (x_{22}/x_{+2}) * 100$	$= (x_{33}/x_{+3}) * 100$		

K and OA were calculated using Equations (6) and (7) respectively [29]:

$$K' = \frac{N \sum_{i=1}^r x_{ii} - \sum_{i=1}^r (x_{i+} * x_{+i})}{N^2 - \sum_{i=1}^r (x_{i+} * x_{+i})}, \quad (6)$$

$$OA = \frac{\sum_{i=1}^r x_{ii}}{N}, \quad (7)$$

where N represents the total number of pixels in the confusion matrix,  $r$  stands for the number of class objects,  $X_{ii}$  denotes the sum of correctly classified pixels in the confusion matrix,  $X_{i+}$  stands for total number of pixels in column I, and  $X_{+I}$  represents the total number of pixels in row  $i$ .

Assessment the temporal change of SAV distribution: after validation of the classification, Landsat-5 and Landsat-8 data were used to map SAV distribution changes for the ten-year period 2008–2018 (Figure 3). MapInfo 12.0 software was used to prepare general SAV distribution mapping for the Khanh Hoa coast, at a scale of 1:50,000, and in more detail for the five study areas, at the scale of 1:25,000.

### 3. Results

#### 3.1. Assessing the Accuracy of Classification Results

The accuracy of image classifying depended not only on sample area selection accuracy but also on the coverage and distribution of SAV. The results achieved on assessing classification accuracies have been listed in Tables 7 and 8 (the confusion matrix for each sensor is shown in the Appendix A).

**Table 7.** The Kappa coefficient and overall classification accuracy for images sourced from three different satellites.

Image	Kappa Coefficient (K)	Overall Accuracy (OA)
VNREDSat-1	0.87	89.40
Landsat-8	0.85	88.27
Sentinel-2	0.84	87.21

**Table 8.** The Producer's accuracy and User's accuracy in estimating the five substrate types (classes) from the three satellites.

Classes	VNREDSat-1		Landsat-8		Sentinel-2	
	Pa (%)	Ua (%)	Pa (%)	Ua (%)	Pa (%)	Ua (%)
SAV	79.02	77.93	79.58	91.87	79.86	92.00
Sandy bottom	97.83	99.26	95.45	88.98	92.86	94.20
Deep water	97.46	100.00	91.53	94.74	88.98	88.98
Mud–sandy bottom	80.36	77.59	87.38	77.59	86.24	79.66
Rock–coral bottom	93.55	94.57	89.80	88.00	88.89	79.28

As shown in Table 7, all satellites were found to be able to provide accurate SAV distribution estimates. The Kappa coefficient and Overall Accuracy accuracies exceeded 0.84 and 87%, respectively, with V1 showing the best results ( $K = 0.87$ ), followed by L8 ( $K = 0.85$ ), and then S2 ( $K = 0.84$ ).

Considering the Pa and Ua coefficients, sandy bottom and deep water were the most accurately identified bottom classes, for all three satellites, achieving both Pa and Ua values  $> 88\%$ . The next most accurate identification was for rock–coral bottom ( $>79\%$ ), followed by detection of mud–sandy bottom, with SAV showing the lowest accuracies, although with both Pa and Ua still better than 77%. The reflected spectrum of sandy bottom and deep water may be higher and less confusing than the others, explaining its higher Pa and Ua values. The reason why SAV achieved the lowest Pa and Ua was that it could be confused with rock–coral or mud–sandy substrates, and if there was algae growing on rocks, dead corals, or several areas with high turbidity, this could lead to similar reflectance spectra between SAV and mud or rock (Appendix A).

### 3.2. Spatial Distribution of SAV in Selected Sections of the Khanh Hoa Coastal Area

The SAV distribution mapping results from L8, S2, and V1 have been depicted in Figure 5, with the SAV areas for each sub-section listed in Table 9. It was found that SAV was mainly distributed in the center of Khanh Hoa province, typical in Nha Trang Bay, with approximately 49.6 ha, and in Nha Phu Lagoon, with 70.1 ha of SAV (using V1 data). The coastal areas to the S and N of the province also showed well-developed SAV resources, with Van Phong Bay, Cam Ranh and Thuy Trieu lagoons showing SAV beds extending over 380.18, 144.4 and 155.5 ha, respectively (using V1 data).

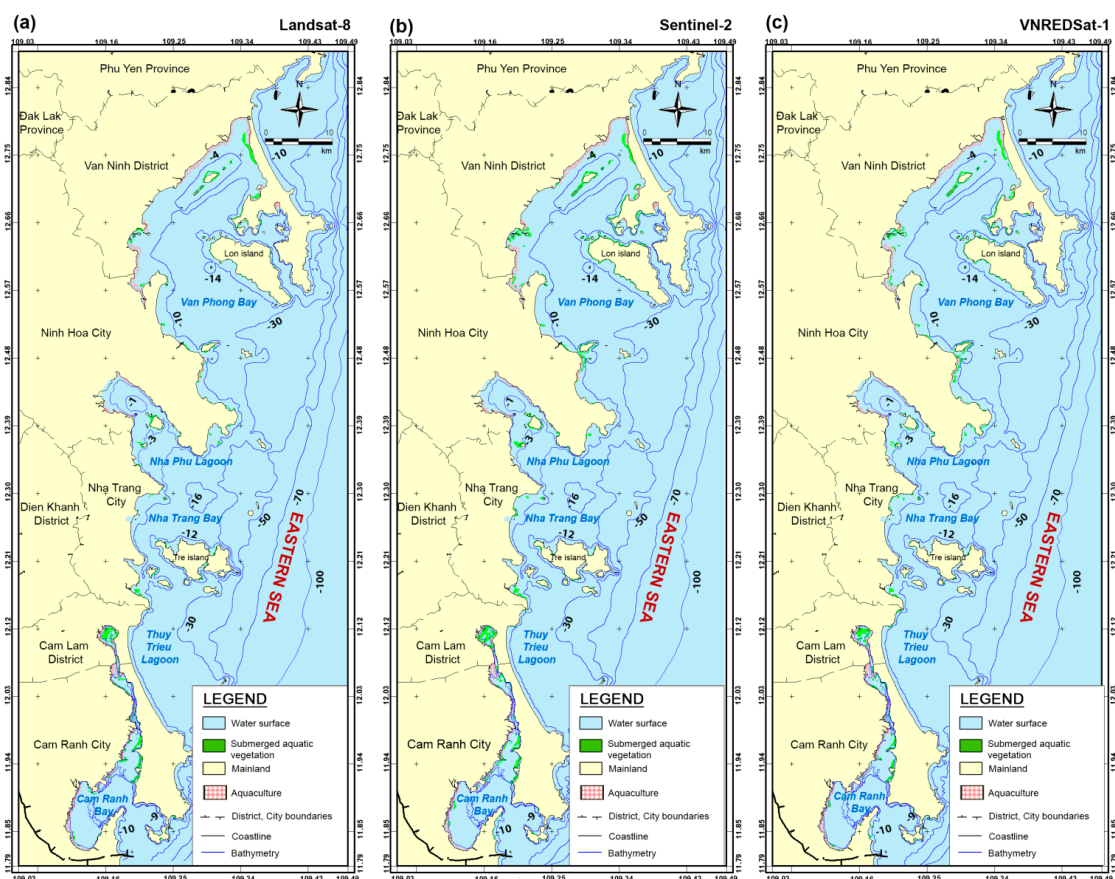


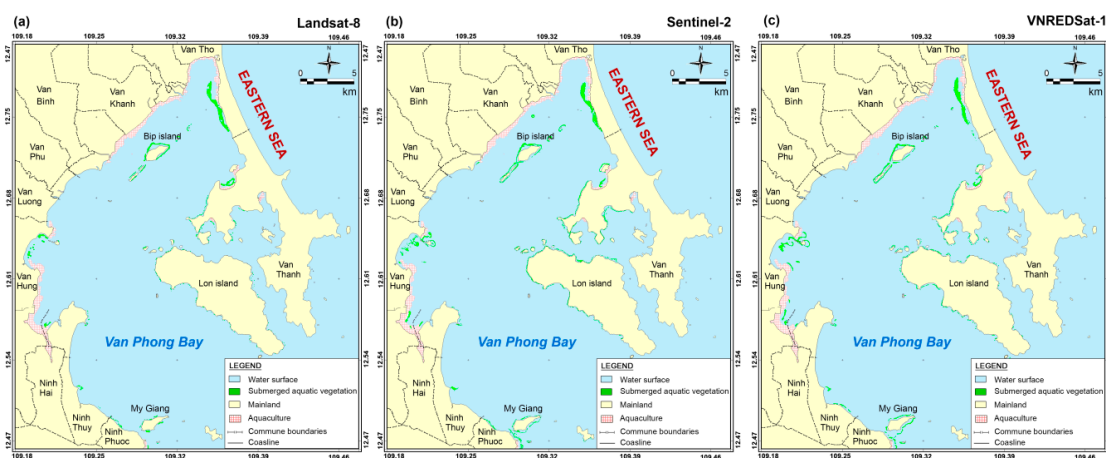
**Figure 5.** SAV distribution maps along the Khanh Hoa coast, created using data from three satellites: (a) Landsat-8 (2018), (b) Sentinel-2 (2019), and (c) VNREDSat-1 (2017).

**Table 9.** SAV areas in Khanh Hoa coastal subsections, determined using data from three satellites.

Location	Submerged Aquatic Vegetation Areas (ha)		
	VNREDSat-1 (2017)	Landsat-8 (2018)	Sentinel-2 (2019)
Van Phong Bay	390.2	270.2	324.2
Nha Phu Lagoon	70.1	63.6	62.6
Nha Trang Bay	49.6	49.8	63.4
Thuy Trieu Lagoon	155.5	209.2	155.3
Cam Ranh Bay	144.4	178.4	193.9
Total	809.8	771.2	799.4

As shown in Figure 5 and in Table 5, the SAV distribution results from the sensors differed slightly. This was particularly true for small areas, such as Nha Phu Lagoon and Nha Trang Bay. The largest SAV distribution area according to the V1 (2017) data was approximately 809.8 ha, whereas S2 (2018) and L8 (2018) data indicated maximum SAV distribution areas of 799.4 and 771.2 ha, respectively (Table 9).

Van Phong Bay: SAV here was usually distributed in shallow water, over a depth range of 0–1.5 m, and could be found over various substrates, including sand, mud–sand, or sand mixed with coral. Seaweed developed to over 5 m on rocky bottoms, or on dead coral. SAV was found to be growing strongly in the coastal areas of Van Tho and Van Thanh cities, with distribution sparser around Ninh Thuy and Ninh Hai cities, and around several small islands (Bip and Lon islands), with total area estimates for the sub-section ranging from 270.2 to 390.2 ha (Figure 6, Table 9). The total acreage reported by the V1 and S2 imagery differed slightly (390.2 ha vs 324.2 ha), while L8 showed a more significant disparity, with a value of 270.2 ha.

**Figure 6.** SAV distribution maps for Van Phong Bay, using data from three satellites: (a) Landsat-8 (2018), (b) Sentinel-2 (2019), (c) VNREDSat-1 (2017).

Nha Phu Lagoon: this sub-section supported the least amount of SAV compared to the other locations in the province, with the SAV mainly distributed around islands—such as Thi, Lao, and Giua islands—with additional small areas observed in the coastal area near Ninh Van city. The total SAV acreages reported for this sub-section ranged from 62.6 to 70.1 ha (Figure 7, Table 9). Several small vegetation beds (smaller than 0.09 ha (1 pixel of L8)), were not reported in the L8 data, while they were detected by both the S2 and V1 platforms. This emphasized the importance of spatial resolution for detecting small SAV beds, with the L8 spatial resolution being lower than both S2 and V1, and this issue became most apparent in the SAV distribution reported around Giua, Lang, and Nua islands. The total SAV acreage and distribution reported for this sub-section by the three satellites were very similar, ranging from 62.6 (S2) to 70.1 ha (L8).

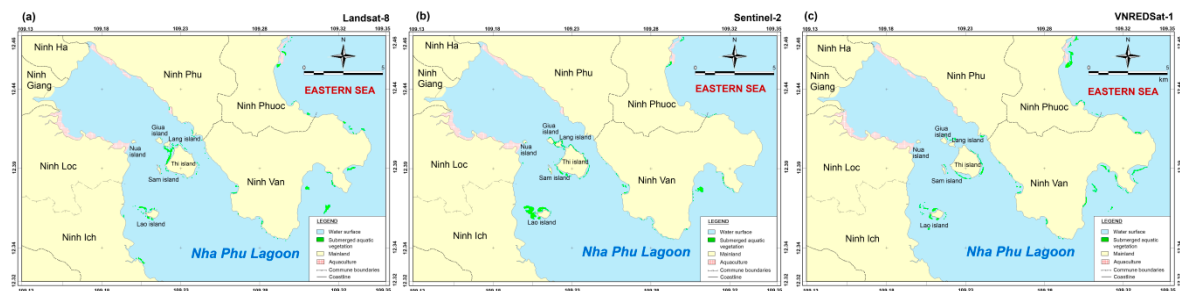


**Figure 7.** SAV distribution maps for Nha Phu Lagoon, using data from three satellites: (a) Landsat-8 (2018), (b) Sentinel-2 (2019), (c) VNREDSat-1 (2017).

Nha Trang Bay: SAV was shown as being distributed in the shallows and around the islands in this sub-section (Figure 8), mainly around Vinh Hai ward, Phuoc Dong city, and Tre Island. Small SAV areas were also reported in the shallows (depth from 1.5–3 m) around Mieu, Mun, Mot, and Tam islands. The total SAV area reported ranged from 49.6 (V1) to 63.4 ha (S2), as shown in Table 9. Similarly to Nha Phu lagoon, several small vegetation beds in this sub-section (<0.09 ha) were not reported by L8.

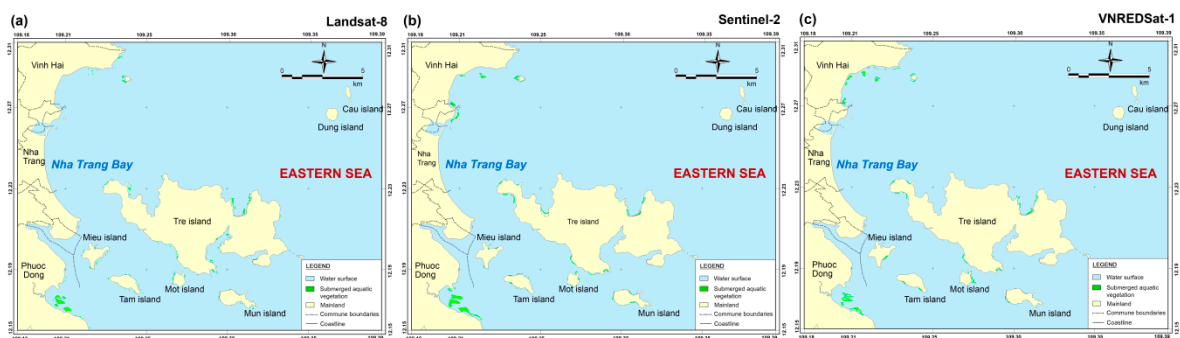


**Figure 8.** SAV distribution maps for Nha Trang Bay, using data from three satellites: (a) Landsat-8 (2018), (b) Sentinel-2 (2019), (c) VNREDSat-1 (2017).

Thuy Trieu Lagoon: Rhodophyta were found to dominate this area, being distributed together with SAV, creating mixed seaweed and seagrass vegetation beds. The SAV was reported to be concentrated mainly in the upper (N) reach of the lagoon, constituting dense beds, with this area consisting of shallow water (0–1.5 m), with mud or mud–sand substrates, around Cam Hoa, Cam Hai Dong, Cam Thanh Bac, and Cam Phuc cities (Figure 9). The total reported acreage of seagrass beds in the lagoon was approximately 155.5 ha (V1) (Table 9). The SAV acreages and distribution reported by the three satellites differed at the northern head of the lagoon, while distribution records for other sub-section localities, including Cam Hai Dong, Cam Thanh Bac, and Cam Duc cities, showed no noticeable differences. The N area of the lagoon showed high turbidity, which made it difficult to estimate SAV distribution, and was probably the cause of the varying SAV acreage and distribution estimates here (Table 9).

Cam Ranh Bay: in this sub-section, SAV distribution was restricted to shallow waters and the area around Binh Ba Island (Figure 10), with an estimated total acreage of 144.4 ha (V1 image, Table 9). In the coastal areas, SAV was mainly found near Cam Hai Dong city, while around Binh Ba Island, it was concentrated in a few small beds off the N end of the island. The SAV bed acreage estimates for this sub-region varied between the satellites, ranging from 144.4 (L8) to 193.9 ha (S2). SAV distribution reports were relatively consistent between the satellites (Figure 10).



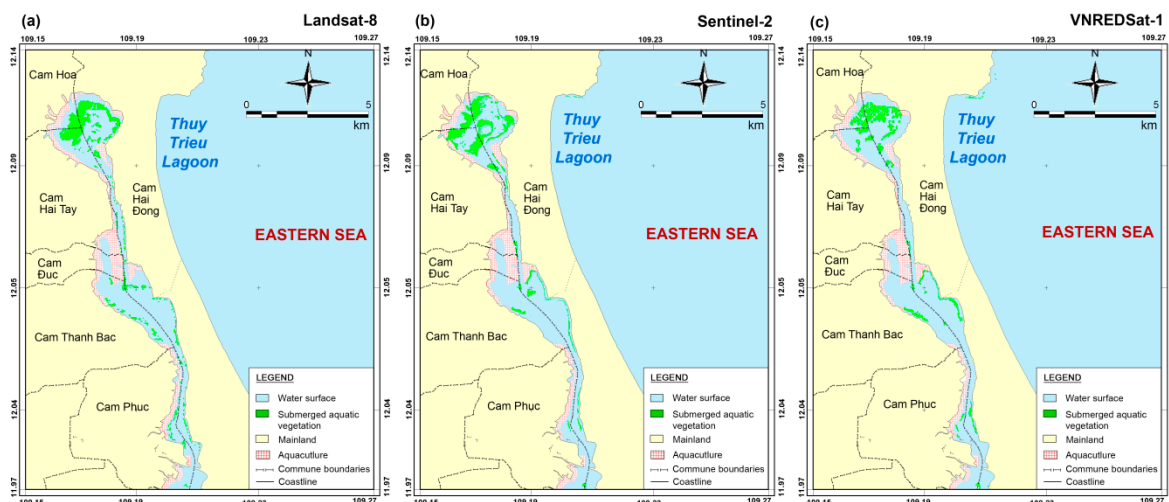


**Figure 9.** SAV distribution maps for Thuy Trieu Lagoon, using data from three satellites: (a) Landsat-8 (2018), (b) Sentinel-2 (2019), (c) VNREDSat-1 (2017).

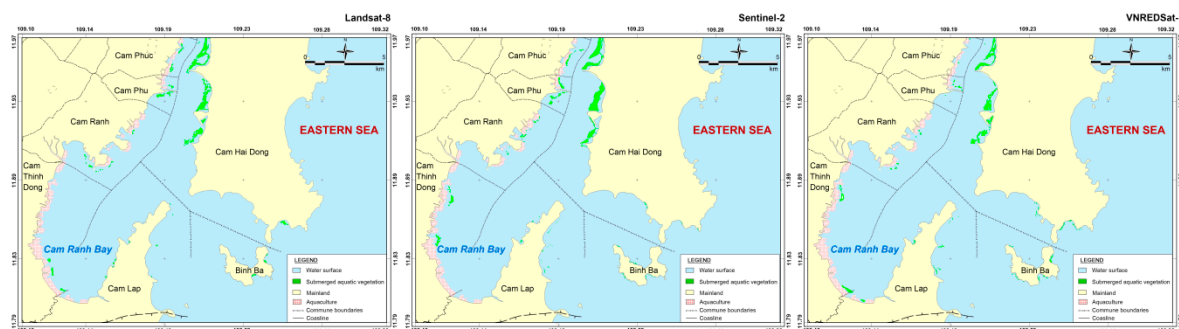


**Figure 10.** SAV distribution maps for Cam Ranh Bay, using data from three satellites: (a) Landsat-8 (2018), (b) Sentinel-2 (2019), (c) VNREDSat-1 (2017).

### 3.3. Assessment of the Temporal Changes to SAV in the Khanh Hoa Area

We compared data from Landsat-5 (2008) and L8 (2018) to study variations in SAV distribution and acreage, with the results listed in Table 10 and illustrated in Figure 11.

**Table 10.** SAV area change over the period 2008–2018, estimated using data from Landsat 5 and 8.

Location	Submerged Aquatic Vegetation Area (ha)					
	Landsat-5 (2008)	Landsat-8 (2018)	Unchanged	Gained SAV	Lost SAV	Average Lost (ha/year)
Van Phong Bay	424.5	270.2	85.9	184.2	338.5	33.9
Nha Phu lagoon	144.3	63.6	15.3	48.3	129.0	12.9
Nha Trang Bay	110.2	49.8	16.1	33.7	94.1	9.4
Thuy Trieu lagoon	345.3	209.2	120.2	89.0	225.1	22.5
Cam Ranh Bay	282.7	178.4	100.1	78.3	182.6	18.3
<b>Total</b>	<b>1307.0</b>	<b>771.2</b>	<b>337.7</b>	<b>433.5</b>	<b>969.3</b>	<b>97</b>

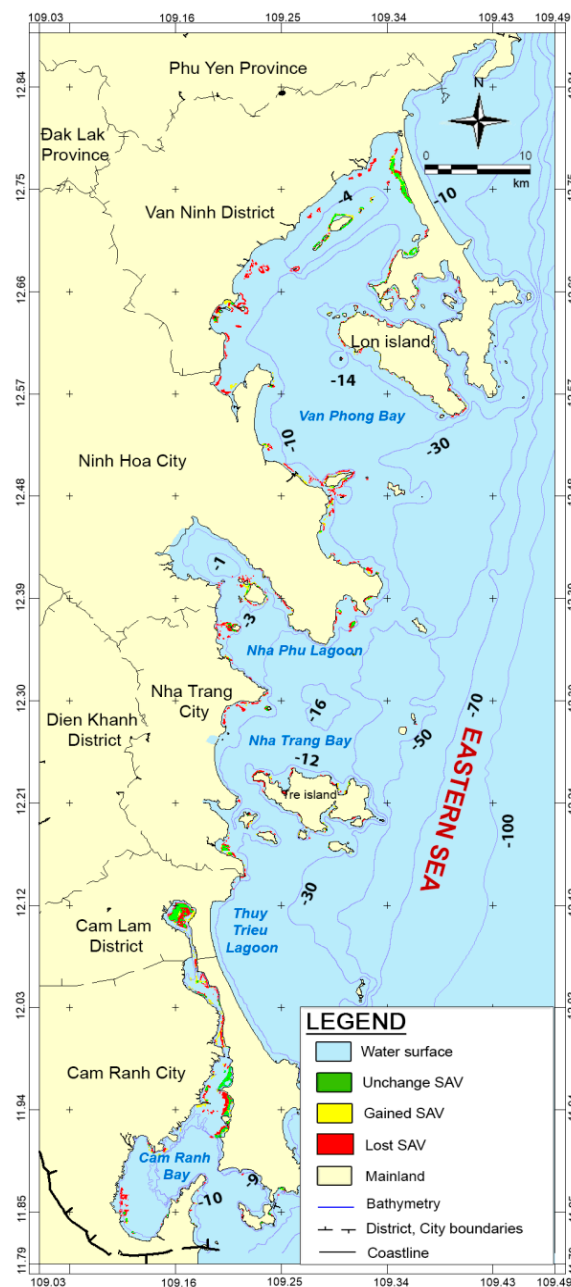


**Figure 11.** SAV change map in the Khanh Hoa coastal area for the period 2008–2018. Estimates were developed using data from Landsat-5 (2008) and Landsat-8 (2018).

The total SAV area along the Khanh Hoa coast, in 2008, was approximately 1307 ha, which had decreased to 771.2 ha, by 2018 (Table 10). Van Phong Bay lost the most SAV, with a decline of 338.5 ha, at an average annual loss rate of 33.9 ha. The other regions which lost SAV included Van Phong Bay, in the Van Ninh coastal area, and My Giang, Thuy Trieu and Cam Ranh bays, with losses of 225.1 ha and 182.6 ha, respectively. In Nha Phu Lagoon and Nha Trang Bay, the area of SAV lost was 5–8 times greater than the area gained.

Over the period 2008–2018, the Khanh Hoa coastal area lost approximately 74.2% of its SAV, in term of acreage, corresponding to a loss of 969.3 ha, while it gained new SAV beds covering just 33.2% (433.5 ha), compared with 2008 coverage. The SAV area gains constituted less than half of SAV area losses in the Khanh Hoa coastal zone.

The average annual SAV acreage lost in the area has been 97 ha. In general, the losses tended to occur in the shallows and along shorelines in areas such as the Van Ninh district (Van Phong), Nha Trang city and from Cam Ranh city, My Giang (Van Phong Bay).

## 4. Discussion

### 4.1. Assessing the Accuracy

The V1 data had the highest Kappa coefficient and accuracy for SAV area classification ( $K = 0.87$ ;  $OA = 89.40$ ), while the lowest results were for S2 ( $K = 0.84$ ;  $OA = 89.40$ ). On the other hand, when the SAV Pa and Ua results for the three sensors were reviewed, S2 imagery performed better, with the highest values ( $Pa > 92\%$ ;  $Ua > 79\%$ ) while V1 exhibited the lowest accuracy ( $Pa > 79\%$ ;  $Ua > 77\%$ ). In general, the accuracy results of three data are relatively high with the water column correction method. This method can be applied to several coastal areas in central Vietnam which have similar climatic and hydrological conditions, such as Quang Nam, Quang Ngai, Binh Dinh, Phu Yen, Khanh Hoa, Ninh Thuan, and Binh Thuan.

Several studies have established SAV coverage with a high degree of accuracy. These include Yang et al. (2006), who mapped Xincun Bay, China, using QuickBird and China-Brazil Earth Resources Satellite (CBERS) satellite data, achieving 85% overall accuracy [46], while Ha (2010) classified ALOS AVNIR-2 imagery, achieving an accuracy of 81.8% in Lap An lagoon [25], and Manuputty et al. (2017) developed a status map in Kotok, Indonesia, with an accuracy of 84%, using WorldView-2 imagery [22]. Compared with these works, the present study achieved a higher level of accuracy, by using data from three different satellites. It is also quite likely that our use of the water column correction method (Lyzenga, 1981) contributed to the accuracy of our results, and it appears that it would be appropriate to use this correction when SAV mapping in our region.

Environmental factors such as turbidity, depth, and waves influence the outputs of satellite data processing and classification [22,47,48]. High turbidity is an important factor, as the intensity of light decreases very quickly with depth, making it harder to detect SAV. Khanh Hoa coastal waters are affected by high turbidity continental water streams, and, based on the Jerlov (1964) seawater clarity level assessment scale [12], the coastal waters in Khanh Hoa province could be divided into two groups: medium turbidity (including Van Phong, Nha Trang, and Cam Ranh bays), and high turbidity (including Nha Phu, and Thuy Trieu lagoons). Nha Phu Lagoon showed higher turbidity, making it harder to estimate SAV presence and distribution than it was in other areas. This caused our Kappa coefficients and accuracy levels to be lower than those reported in several other SAV distribution studies around islands. These included Hoang et al. (2015), with a classification accuracy of 98.3% and Kappa coefficient of 0.96, in Rottneest Island, Western Australia [21], and Nguyen (2015) in Ly Son Island, Quang Ngai province, Vietnam, with high classification accuracy and Kappa coefficients of 94 % and 0.93, respectively [24].

In this study, the Kappa coefficient was higher for L8 ( $K = 0.85$ ) than it was for S2 ( $K = 0.84$ ), showing that spatial resolution was not always the answer for improving classification accuracy. It was of interest to note, however, that Konstantinos et al. (2016) compared S2 and L8 data around Lesvos Island, Greece when estimating SAV status, and showed that using S2 significantly improved the SAV classification accuracy, compared to L8, with a Kappa coefficient of 0.9 [27]. The authors did not need to include any water column correction, since the waters near Lesvos Island were very clear, which facilitated SAV detection.

### 4.2. Factors Influencing Interpretation Processes

In general, the classification outputs for bottom types that were established using the Lyzenga (1981) water column correction method showed high levels of accuracy, but the classification process developed some erroneous classifications. These may have originated from different factors. Firstly, the average spatial resolution of the three satellites—L8 (30 m), S2 (10 m), and V1 (10 m)—were

not high enough to allow detection of SAV areas < 0.01 ha. Moreover, there was a one year discrepancy between the timing of our field surveys and the selected S2 and V1 satellite imagery. This difference led to a few discrepancies in interpretation processing, even though it did not lead to noticeable differences between the closely timed imagery.

Environmental factors such as turbidity, depth, the spatial resolution of the remote sensing images, and satellite sensor sources were also factors capable of influencing classification results [17,24,27]. Figure 12 is an illustration of how satellite spatial resolution could affect SAV estimation, using two typical shapes (points and regions) for L8, S2, and V1 imagery for Khanh Hoa province. In this figure, it is apparent that smaller pixel sizes led to better characterization of fine scale water bodies, and so to more detailed SAV distribution results. These results showed that spatial resolution plays an important role in coastal substrate characterization accuracy.

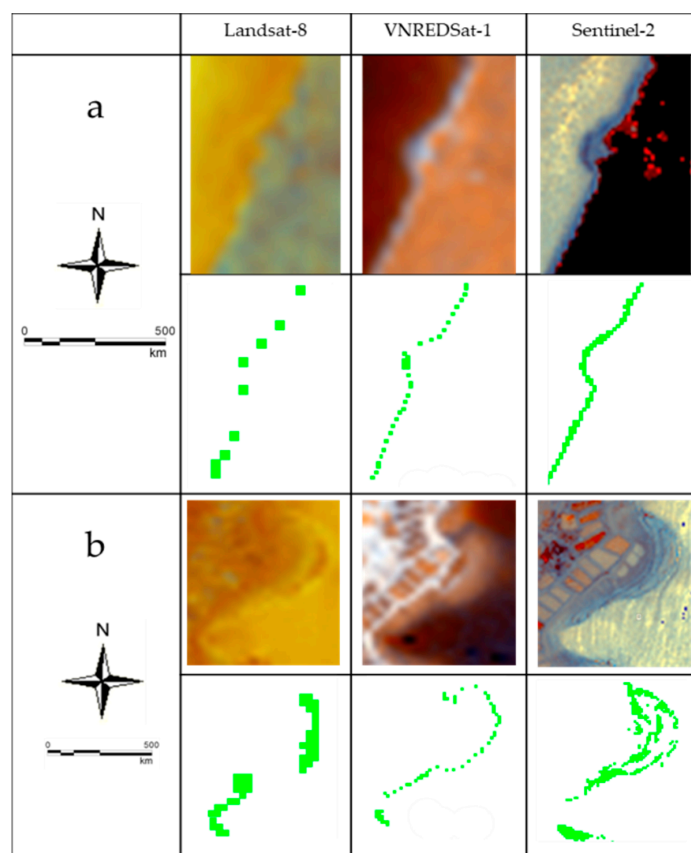


**Figure 12.** Examples of point and polygon SAV classifications using Landsat 8, Sentinel-2, and VNREDSat-1 imagery from the Khanh Hoa coastal area. The imagery depicts SAV areas in (a) Van Phong Bay, and (b) My Giang, Nha Phu Lagoon.

For SAV mapping, misclassification usually relate to the impact of the mixed substrate. The lower classification accuracy from L8 data might due to situations where the spatial SAV extent was smaller than its pixel size, leading to unrecognized SAV, and confusion over rock–coral or mud–sandy bottoms that hosted small SAV patches. Over-classification in S2 was caused by mixed SAV, rock, and water reflections within a pixel. Meanwhile, the Kappa coefficient and OA for L8 were higher than those for S2 (Table 3), and this was thought to be due to the difference of satellite sensor spectral bands. These issues illustrated that spatial resolution was not the only influencing factor for SAV estimation and substrate type classification in the study area.

All three satellites had blue bands, which were better for detecting sunlight transmission through the water column than others [12,40,49]. The S2 coastal band could penetrate even better than the blue band, but was not used in this study due to its 60 m spatial resolution, which was more appropriate

for the general resolution of S2 data. Hence, bands comprising blue, red, and green were applied to water column correction for two of the image sources (V1 and S2), while the coastal, blue, and green bands from L8 imagery were used (Table 5).

V1 and S2 had the same resolution as well as the same bands, and their initial prediction results showed good similarity; however, V1 achieved the best output accuracy assessment, while S2 achieved the lowest value (Table 7). This result probably occurred because V1 has a spatial resolution of 10 m and the band pairs correlation coefficient was quite high ( $R^2 > 0.9$ ), making the V1 bottom classification accuracy higher than it was for L8 or S2 (Tables 7 and 8). L8 had a lower spatial resolution (30 m), potentially causing less detail to be available than for V1—and its accuracy was correspondingly lower. Although L8 had a lower spatial resolution than the other two imagery sources, the image collection time coincided with our survey time (L8 imagery was acquired in May 2018, and field surveys were conducted in June and October 2018), and the L8 Kappa coefficient was higher than that of S2. Furthermore, the S2 spectral band pairs correlation coefficient was lower than the other image sources ( $0.93 > R^2 > 0.56$ ), meaning its band pairs DII index was relatively poor, leading to reduced accuracy.

Apart from its advantages in substrate classifying, V1 had a limitation in that, unlike L8 and S2, it has no coastal band—and so could not acquire information on deep water in coastal areas. In addition, this is a small satellite type, with a comparatively small image size ( $17.5 \times 17.5$  km) [34,35]. While Landsat only used two scenes and S2 needed three images, to cover the study area, V1 required nine images, each covering a small area and making it difficult to collate all the imagery needed to cover the Khanh Hoa coast. Moreover, due to the larger number of images, it took much longer to process the V1 imagery than it did for the larger L8 and S2 imagery.

In this study, optical data analyzing satellite imagery were used to map SAV distribution and temporal change. This method effective for mapping broad areas but it limited to deep waters due to light attenuation in waters [50,51]. So, the scope of the study is shallow waters, which was  $< 10$  m deep. Several other methods can detect the distribution of SAV living  $> 10$  m deep, such as the multibeam echosounder and the side scan sonar. These methods can map SAV depth variations with a large range from 0 to 25 m [50,52].

Besides this drawback, the optical data also depends on the weather, clouds, rain, seasons, and day or night [51–53]. This is difficult for collecting satellite data to detect seasonal changes subjects such as SAV. Because of the method limitation, the study was unable to collect three data sources in the same months of one year. At present, there are very few studies on seasonal variation of SAV or the growth of seasonal SAV in Vietnam in particular and Khanh Hoa in general. May-Lin et al. (2013) studied the seasonal rate of *Sargassum* species at Port Dickson, Malaysia show that the monthly mean growth rates with two periods of high growth rates (January–February, and June–July), which mean that *Sargassum* in the phase of increasing and stabilization biomass [53]. The climate of Malaysia which is a tropical rainforest climate is similar to the climate of Vietnam. This led to similarities in the growth and coverage characteristics of SAV between Vietnam and Malaysia. Another study by Pham (2006) on the variation of seagrass population in the Khanh Hoa coast also shows that the density, above-ground biomass, leaf growth rate and leaf production of seagrass beds were often high in the dry season and often low in the rainy season. In the period May–August, seagrass in the Khanh Hoa coast in the phase of stabilization biomass includes the late-growth and reproduction stage [54]. Therefore, the growth and coverage characteristics of SAV can be assessed to be similar and were no significant variation in the dry season, which can be easily detected to SAV distribution in this period.

In addition to environmental factors and satellite sensor sources, the interpretation process of SAV was also dependent on the classification method [55,56]. In this study, the maximum likelihood classifier (MLC) algorithm was applied for substrate type classification. However, when the boundaries of SAV and other benthic habitats are not well defined, the linear discrimination functions of the MLC may not work [55]. Besides, conditions of the MCL method require large amounts of training samples and equal covariance, which may result in misclassification between SAV and other benthic

habitats [55,57]. The recent technique advances on machine learning (ML) can improve these limitations and encourage new approaches for SAV maps over various time scales. When comparing traditional MCL and ML method including random forests, rotation forests, and canonical correlation forests for SAV mapping using Sentinel-2, Nam et al. (2020) revealed that the ML method outperformed the MLC [55]. Similarly, Pham et al. (2019) also reviewed the limitations of the MLC method and suggested ML techniques for mapping coastal vegetation [57]. Although ML techniques have several benefits, the application of this method is infancy in the field of SAV map [55,57]. Thus, a variety of algorithms with the development of ML techniques using for multi-source remote sensing image applied SAV mapping should be encouraged for future studies.

The interpretation processes are affected by a number of factors, so this study has some limitations. However, this study could be one of the fundamental studies and the first of multi-source remote sensing data about the assessment of SAV distribution in the coastal areas in Khanh Hoa province and central Vietnam.

#### 4.3. Temporal Changes to SAV Distribution

Other studies have quantified SAV distribution elsewhere along the Vietnamese coast, and comparisons show that our study area had less SAV than the Quang Ninh coastal area (1450 ha), and more than both the Hai Phong (490 ha) and Quang Binh coastal areas (350 ha) (Cao, 2014). The results from this study mean that SAV distribution in the Khanh Hoa coastal zone can now be recognized as one of the most extensive along the Vietnamese coast.

In Cam Ranh Bay, the SAV distribution area estimate found in this study was lower than that of Chen et al. (2015), who estimated that there was approximately 195.3 ha between Cam Hai Dong and Cam Phuc cities, for 2015 (Table 11). They also reported that an SAV decrease over the period 1996 to 2015 was caused by encroachment of aquaculture-based activities [26]. This encroachment continued between 2015 and 2019, explaining why our SAV estimate for this location was lower still than theirs from 2015.

**Table 11.** Comparison of SAV distribution in Khanh Hoa coastal obtained in this study with the literature.

Location \ Area (ha)	This Study (2018)	Other Studies	References
Van Phong Bay	270.2	600 (2013)	Nguyen et al. [10]
Nha Phu lagoon	63.6	-	-
Nha Trang Bay	49.8	68 (2015)	Nguyen et al. [15]
Thuy Trieu lagoon	209.4	547 (2012)	Nguyen et al. [9]
Cam Ranh Bay	178.4	195.3 (2014)	Chen et al. [26]
Total	771.2	-	-

Our findings for Nha Trang Bay were quite similar to those of Nguyen et al. (2015), with values of 49.8 and 68 ha, respectively. Nguyen et al. (2015), reported that, in 2015, SAV was distributed mainly around Phuoc Dong and Hon Tre city, and over several small regions (under 1 ha) around Mieu, Mun, and Mot islands [15].

Nguyen et al. (2012) studied wetland ecosystems in Thuy Trieu Lagoon, and assessed an SAV acreage of approximately 547 ha; two years later, Nguyen et al. (2014) estimated that SAV beds in Van Phong Bay covered approximately 600 ha [9]. In comparison with the results from these two studies (Nguyen et al. (2012, 2014), our results for the same areas were much lower (Table 11).

#### 4.4. Temporal Changes in SAV Extent

After assessing the overall accuracy and Kappa coefficients, all three images had relatively high quality outputs, making it possible to establish SAV distribution status in the study area. Although V1 data gave the best results for substrate classification, as it was only launched in 2013, earlier data

was not available [34,35]. Therefore, selecting Landsat gave us the advantages of not only high levels of accuracy, but also a longer data record than was available from either S2 or V1.

According to Pham (2006), and hydrological–coastal environment data (2003) in the Khanh Hoa province in particular, and Central Vietnam in general, the growth and coverage characteristics of SAV do not change significantly in the dry season, especially from May to August, SAV in the Khanh Hoa coast in the phase of increasing and stabilization biomass [54,56]. Therefore, this study have selected the best quality images in the dry months to conduct the interpretation of SAV temporal changes.

In 2008, several decisions of the government approving the overall planning on the socio-economic development of Central Vietnam up to 2020 focus on economic development to build the coastal economic infrastructure, comprising the system of seaports, Van Phong international entropot port, and tourist development including water sports tourism, coastal landscape tourism and so on [58]. This allowed us to select historical Landsat-5 imagery from 2008 to assess the extent of SAV changes over the last 10 years.

Khanh Hoa coastal waters have lost approximately 969.3 ha of SAV over the 10 year period 2008–2018, at an average annual loss of ~97 ha. Generally, the losses occurred in shallow water, near shorelines which could be directly impacted by human activities [8,15,26,27].

Our findings were in accord with those of several previous studies, including Nguyen et al. (2013), who studied SAV degradation in Van Phong Bay. The identified reasons included damage caused by locals, who continually dug into the SAV areas with hoes, looking for oysters and mussels, and by the developing economic sector, with port and ship repair infrastructure such as the Hyundai Vinashin factory having negative effects on the adjacent SAV beds [9,10]. Similarly, Chen et al. reasoned that SAV acreage changes in Cam Ranh Bay were caused by infrastructure and aquaculture developments there [26].

Nguyen et al. (2014) noted that degradation of SAV beds in Thuy Trieu Lagoon was caused by locals digging on them for shellfish, and by the encroachment of tourism infrastructure buildings [9]. As an example, the Vinpearl Land resort involved golf course construction, which brought about the loss of 18 ha of seagrass from the area [9,15]. In general, SAV acreage has been reduced by various human activities, including overexploitation of marine resources, shellfish collection, shrimp pond construction, tourism, and seaport development, leading to a remarkable reduction in regional SAV [10,15,26].

## 5. Conclusions

In this study, the authors evaluated the performance of the V1 sensor for detection of SAV along the coast of Khanh Hoa province, Vietnam, and compared its results to those achieved using S2 and L8 satellite sensors. This has been the first study to apply V1 data to establish SAV distribution status, and the results showed that all three satellite sensors had relatively high levels of accuracy ( $K > 0.83$ ), and could be used to prepare SAV distribution maps. The L8 Kappa coefficient and overall accuracy reached 0.85 and 88.27%, respectively, which were better than those achieved by the S2 ( $K = 0.84$ ;  $OA = 87.21\%$ ) and V1 sensors ( $K = 0.87$ ;  $OA = 89.40\%$ ).

The SAV bed distribution status results from the three satellites showed differences that were centered around several small areas, such as Nua, Lao, and Rua islands. Regarding the SAV acreage estimates for the study area, the estimate were broadly similar, ranging from 771.2 to 809.8 ha, with Van Phong Bay hosting the largest acreage, at ~390.2 ha (V1). Over the period 2008–2018, SAV declined significantly across the study area, with approximately 74.2% of its area lost, with replacement areas limited to less than half of this. SAV was seen to have almost disappeared from many shallow areas and from locations close to the shore, to the extent that the overall SAV area decreased in the study area at an annual average rate of ~97 ha.

Currently, there are no studies using V1 data for coastal resource monitoring and management, with this being the first study to apply V1 data to SAV detection in coastal waters—with the results exhibiting high classification accuracy, and demonstrating its potential in this field. To enhance the applicability of remote sensing technology in Vietnam, it will be important to continue studying

and applying V1 data to map SAV distribution around islands and in coastal areas. It would also be beneficial to examine the application of V1 to the determination of SAV species composition, coverage, and dried biomass, thus establishing an even better understanding of the application of satellite-sourced data to SAV studies.

This work has identified that V1 imagery has an important shortcoming, in that the area captured in each scene is relatively small, making development of SAV distribution maps for large coastal areas complex and time-consuming. This suggests that it would be beneficial to combine V1 data with that of other satellites, such as WorldView-2, BKA, THAICHOTE, SSOT, ALSAT-2, and so on, in an effort to overcome this limitation.

**Author Contributions:** Conceptualization, Tran Ngoc Khanh Ni, Hoang Cong Tin, Vo Trong Thach, Cédric Jamet and Izuru Saizen; Funding acquisition, Hoang Cong Tin and Vo Trong Thach; Investigation, Tran Ngoc Khanh Ni, Hoang Cong Tin and Vo Trong Thach; Methodology, Tran Ngoc Khanh Ni, Hoang Cong Tin, Cédric Jamet and Izuru Saizen; Supervision, Hoang Cong Tin and Izuru Saizen; Validation, Tran Ngoc Khanh Ni, Hoang Cong Tin, Vo Trong Thach, Cédric Jamet and Izuru Saizen; Writing—original draft, Tran Ngoc Khanh Ni, Hoang Cong Tin and Vo Trong Thach; Writing—review & editing, Cédric Jamet and Izuru Saizen. All authors have read and agreed to the published version of the manuscript.

**Funding:** This study was funded by Vietnam National Foundation for Science and Technology Development (Nafosted) (grant number 106.06-2017.340) and Vietnam Academy of Science and Technology (project code VT-UD.01/17-20) belonging to National Program on Space Science and Technology (2016–2020).

**Acknowledgments:** The authors would like to thank Faculty of Environmental Science, University of Sciences, Hue University and the Coastal & Marine Environment Research team members for their support with experiments and assistance in the field while collecting samples.

**Conflicts of Interest:** The authors declare no conflict of interest.

## Appendix A. Evaluation Accuracy after Classification

**Table A1.** Landsat-5 confusion matrix table (2008).

Layers	SAV	Sand	Deep Water	Mud	Rock–Coral	Total	UA
SAV	<b>103</b>	0	0	16	1	120	85.83
Sand	0	<b>130</b>	4	0	0	134	97.01
Deep water	0	0	<b>106</b>	4	6	116	91.38
Mud	30	0	6	<b>92</b>	3	131	70.23
Rock–Coral	11	3	0	2	<b>90</b>	106	84.91
Total	<b>144</b>	<b>133</b>	<b>116</b>	<b>114</b>	<b>100</b>	607	
PA	71.53	97.74	91.38	98.57	80.36		OA 85.83

Overall accuracie (OA), user accuracie (UA), and producer accuracies (PA); Kappa coefficient 0.82.

**Table A2.** VNREDSat-1 confusion matrix table (2017).

Layers	SAV	Sand	Deep Water	Mud	Rock–Coral	Total	UA
SAV	<b>113</b>	2	3	21	6	145	77.93
Sand	0	<b>135</b>	0	1	0	136	99.26
Deep water	0	0	<b>115</b>	0	0	115	100.00
Mud	25	1	0	<b>90</b>	0	116	77.59
Rock–Coral	5	0	0	0	<b>87</b>	92	94.57
Total	<b>143</b>	<b>138</b>	<b>118</b>	<b>112</b>	<b>93</b>	604	
PA	79.02	97.83	97.46	80.36	93.55		OA 89.40

Kappa coefficient 0.87.



**Table A3.** Landsat-8 confusion matrix table (2018).

Layer	SAV	Sand	Deep Water	Mud	Rock–Coral	Total	UA
SAV	113	0	0	7	3	123	91.87
Sand	4	130	2	0	7	143	90.91
Deep water	0	0	108	6	0	114	94.74
Mud	22	0	4	95	0	121	78.51
Rock–Coral	3	8	4	0	88	103	85.44
Total	142	138	118	108	98	604	
PA	79.58	94.20	91.53	87.96	89.85		OA 88.41

Kappa coefficient: 0.85.

**Table A4.** Sentinel-2 confusion matrix table (2019).

Layers	SAV	Sand	Deep Water	Mud	Rock–Coral	Total	UA
SAV	115	2	0	6	2	125	92.00
Sand	3	130	0	2	3	138	94.20
Deep water	3	0	105	7	3	118	88.98
Mud	18	0	3	94	3	118	79.66
Rock–Coral	5	8	10	0	88	112	79.28
Total	144	140	118	109	99	610	

Kappa coefficient: 0.84.

## References

- Dai, N.H. Seagrass in Vietnam. In *Seagrasses: Resource Status and Trends in Indonesia, Japan, Malaysia, Thailand and Vietnam*; Seizando-Shoten: Tokyo, Japan, 2011; pp. 12–53.
- Nguyen, V.T.; Nguyen, D.T.; Nguyen, H.D. *Vietnamese Seagrasses and Seaweeds (in Vietnamese)*; The Sciences and Technology Press: Ha Noi, Vietnam, 2005.
- Huynh, Q.N.; Nguyen, H.D. The seaweed resources of Vietnam. In *Seaweed Resources of the World*; Critchley, A.T., Ohno, M., Eds.; Japan International Cooperation Agency: Yokosuka, Japan, 1998; pp. 62–69.
- Lobban, S.; Harrison, P.J. *Seaweed Ecology and Physiology*; Cambridge University Press: Vancouver, BC, Canada, 1977.
- Mark, D.S.; Susan, R.; Carmen, L.; Imen, M.; Lynne, Z.H.; Christine, C.S.; Michael, W.B. The role of ecosystems in coastal protection: Adapting to climate change and coastal hazards. *Ocean Coast. Manag.* **2014**, *90*, 50–57.
- Tien, N.V. *Resources of Vietnamese Seagrass (in Vietnamese)*; Hanoi University of Science and Technology: Ha Noi, Vietnam, 2013.
- Trang, T.T.M.; Ha, N.T.N.; Thanh, T.D. Position resources in the coastal area of Khanh Hoa province: Potential and prospects. *J. Mar. Sci. Technol.* **2015**, *15*, 13–24. [[CrossRef](#)]
- Dai, N.H.; Tri, P.H.; Linh, N.T.; Vy, N.X. The degradation of seagrass beds in Khanh Hoa province and the ability of restoration of these meadows (in Vietnamese). In Proceedings of the Scientific Conference of “BIEN DONG-2002”, Nha Trang, Vietnam, 16–19 December 2002.
- Hoa, N.X.; Thuy, N.N.N.; Hieu, N.T. Current status of mangroves and seagrasses in Thuy Trieu lagoon, Khanh Hoa province (in Vietnamese). In Proceedings of the Fifth National Scientific Conference on Ecology and Biological Resources, Ha Noi, Vietnam, 18 October 2013; pp. 488–496.
- Hoa, N.X.; Thuy, N.N.N. Current status and trends of mangroves and seagrasses in Van Phong Bay, Khanh Hoa province (in Vietnamese). *Collect. Mar. Res. Work.* **2014**, *20*, 135–147.
- Kerr, J.T.; Ostrovsky, M. From space to species: Ecological applications for remote sensing. *Trends Ecol. Evol.* **2003**, *18*, 299–305. [[CrossRef](#)]
- Edwards, A.J. *Remote Sensing 2004: Handbook for Tropical Coastal Management*; United Nations Educational, Scientific and Cultural Organization: Paris, France, 2004.

13. Green, E.P.; Mumby, P.J.; Edwards, A.J.; Clark, C.D. A review of remote sensing for the assessment and management of tropical coastal resources. *Coast. Manag.* **1996**, *24*, 1–40. [[CrossRef](#)]
14. Hashim, M.; Abdullah, A.; Rasib, A.W. Integration of remote sensing-GIS techniques for mapping seagrass and ocean colour off Malaysian Coasts. In Proceedings of the Asian Conference on Remote Sensing, Kuala Lumpur, Malaysia, 20–24 October 1997.
15. Hoa, N.X.; Thuy, N.N.N.; Hieu, N.T. Current status and trends of mangroves and seagrasses in Nha Trang Bay, Khanh Hoa province (in Vietnamese). *Collect. Mar. Res. Work.* **2015**, *21*, 201–211.
16. Qihao, W. *Remote Sensing and GIS Integration, Theories, Methods and Applications*; The McGraw-Hill Companies: New York, NY, USA, 2010.
17. Koedsin, W.; Intararuang, W.; Ritchie, R.J.; Huete, A. An Integrated Field and Remote Sensing Method for Mapping Seagrass Species, Cover, and Biomass in Southern Thailand. *Remote Sens.* **2016**, *8*, 292. [[CrossRef](#)]
18. Gullström, M.; Lundén, B.; Bodin, M.; Kangwe, J.; Öhman, M.C.; Mtolera, M.S.; Björk, M. Assessment of changes in the seagrass-dominated submerged vegetation of tropical Chwaka Bay (Zanzibar) using satellite remote sensing. *Estuar. Coast. Shelf Sci.* **2006**, *67*, 399–408. [[CrossRef](#)]
19. Phinn, S.; Chris, R.; Arnold, D.; Vittorio, B.; Janet, A. Mapping seagrass species, cover and biomass in shallow waters: An assessment of satellite multi-spectral and airborne hyper-spectral imaging systems in Moreton Bay (Australia). *Remote Sens. Environ.* **2008**, *112*, 3413–3425. [[CrossRef](#)]
20. Noiraksar, T.; Sawayama, S.; Phauk, S.; Komatsu, T. Mapping Sargassum bedsoff the coast of Chon Buri Province, Thailand, using ALOS AVNIR-2 satellite imagery. *Bot. Mar.* **2012**, *57*, 367–377.
21. Hoang, T.C.; O’Leary, M.J.; Fotedar, R.K. Remote-sensed mapping of Sargassum spp. distribution around Rottneest Island, Western Australia, using high-spatial resolution WorldView-2 satellite data. *J. Coast. Res.* **2016**, *32*, 1310–1321.
22. Manuputty, A.; Gaol, J.L.; Agus, S.B.; Nurjaya, I.W. The utilization of Depth Invariant Index and Principle Component Analysis for mapping seagrass ecosystem of Kotok Island and Karang Bongkok, Indonesia. *IOP Conf. Ser. Earth Environ. Sci.* **2017**, *54*, 012083. [[CrossRef](#)]
23. Hoang, T.C.; Phap, H.T.; Tuan, N.Q.; Son, T.P.H. Application of remote sensing and Geographical Information System (GIS) techniques in assessing the existing situation of seagrass meadow at coastal wetland in Huong Phong commune, Huong Tra district, Thua Thien Hue province. *J. Sci. Hue Univ.* **2011**, *65*, 231–239.
24. Nguyen, H.Q.; Luong, V.T.; Ho, D.D. Study on spatial distribution of coral reefs in Ly Son Island using GIS and remote sensing technique. *J. Mar. Sci. Technol.* **2015**, *15*, 264–272.
25. Thang, H.N.; Son, T.P.H. Applying techniques of calculating depth invariant index in mapping the distribution of seagrass beds. *Hue Univ. J. Sci.* **2014**, *92*, 93–104.
26. Chen, C.F.; Lau, V.K.; Chang, N.B.; Nguyen, T.S.; Tong, P.H.S.; Chiang, S.H. Multi-temporal change detection of seagrass beds using integrated Landsat TM/ETM+/OLI imageries in Cam Ranh Bay, Vietnam. *Ecol. Inform.* **2016**, *35*, 43–54. [[CrossRef](#)]
27. Konstantinos, T.; Spyridon, C.S.; Apostolos, P.; Nikolaos, S. The use of Sentinel-2 imagery for seagrass mapping: Kalloni Gulf (Lesvos Island, Greece) case study, Proc. SPIE 9688. In Proceedings of the Fourth International Conference on Remote Sensing and Geoinformation of the Environment (RSCy2016), Paphos, Cyprus, 4–6 April 2016.
28. Eva, K.C.R.; Mitchell, L.; Shihu, Z.; Stuart, P. Seagrass habitat mapping: How do Landsat 8 OLI, Sentinel-2, ZY-3A, and Worldview-3 perform. *Remote Sens. Lett.* **2018**, *9*, 686–695.
29. Khanh Hoa People’s Committee. *Khanh Hoa Geographic Atlas*; National Political Publishing House of Vietnam: Ha Noi, Vietnam, 2003; Volume 8, p. 609.
30. U.S. Geological Survey; U.S. Department of the Interior. *Landsat- Earth Observation Satellites. Fact Sheet 2015–3081, ver. 1.1, August 2016 Supersedes USGS Fact Sheets 2012–3072 and 2013–3060*; Earth Resources Observation and Science Center: Su Falls, SD, USA, 2016.
31. Ilori, C.O.P.N.; Knudby, A. Analyzing Performances of Different Atmospheric Correction Techniques for Landsat 8: Application for Coastal Remote Sensing. *Remote Sens.* **2019**, *11*, 469. [[CrossRef](#)]
32. Pham, Q.V.; Ha, N.T.T.; Pahlevan, N.; Oanh, L.T.; Nguyen, T.B.; Nguyen, N.T. Using Landsat-8 Images for Quantifying Suspended Sediment Concentration in Red River (Northern Vietnam). *Remote Sens.* **2018**, *10*, 1841. [[CrossRef](#)]
33. Sentinel-2A Satellite Sensor. Available online: <https://www.satimagingcorp.com/satellite-sensors/other-satellite-sensors/sentinel-2a/> (accessed on 21 November 2019).

34. Hung, L.V.; Manh, V.P.; Chuc, D.M.; Hung, Q.B.; Thanh, T.N. Comparison of various image fusion methods for impervious surface classification from VNREDSat-1. *Int. J. Adv. Cult. Technol.* **2016**, *4*, 1–6.
35. Tan, D.N. Space technology institute and VNREDSat-1. In Proceedings of the First Steering Committee of The Sentinel Asia Step 3, Ha Noi, Vietnam, 13–15 October 2015.
36. Thao, N.V. *Assessment of Wetland Ecosystems with Remote Sensing Data, Apply the Test to VNREDSat-1 Satellite*; State Science and Technology Program on Space Technology 2012–2015: Ha Noi, Vietnam, 2015.
37. Todd, A.S.; Warren, B.C.; Conghe, S.; Morton, J.C.; Zhiqiang, Y. Radiometric correction of multi-temporal Landsat data for characterization of early successional forest patterns in western. *Remote Sens. Environ.* **2006**, *103*, 16–26.
38. Moran, M.S.; Ray, D.J.; Philip, N.S.; Philippe, M.T. Evaluation of simplified procedures for retrieval of land surface reflectance factors from satellite sensor output. *Remote Sens. Environ.* **1992**, *41*, 169–184. [[CrossRef](#)]
39. ENVI. *FLAASH User's Guide*; Version 4.7; ENVI: Boulder, CO, USA, 2009.
40. Lyzenga, D.R. Passive remote sensing techniques for mapping water depth and bottom features. *Appl. Opt.* **1978**, *17*, 179–338. [[CrossRef](#)] [[PubMed](#)]
41. Lyzenga, D.R. Remote sensing of bottom reflectance and water attenuation parameters in shallow water using aircraft and Landsat data. *Int. J. Remote Sens.* **1981**, *1*, 71–82. [[CrossRef](#)]
42. Blakey, T.; Melesse, A.; Hall, M. Supervised classification of benthic reflectance in shallow subtropical waters using a generalized pixel-based classifier across a time series. *Remote Sens.* **2015**, *7*, 5098–5116. [[CrossRef](#)]
43. Setyawidati, N.; Kaimuddin, A.H.; Wati, I.P.; Helmi, M.; Widowati, I.; Rossi, N.; Liabot, P.O.; Stiger-Pouvreau, V. Percentage cover, biomass, distribution, and potential habitat mapping of natural macroalgae, based on high-resolution satellite data and in situ monitoring, at Libukang Island, Malasoro Bay, Indonesia. *J. Appl. Phycol.* **2017**, *30*, 159–171. [[CrossRef](#)]
44. Congalton, R.G.; Green, K. *Assessing the Accuracy of Remotely Sensed Data: Principles and Practices*; Lewis Publishers: Boca Raton, FL, USA, 1999.
45. Congalton, R.G. A review of assessing the accuracy of classification of remotely sensed data. *Remote Sens. Environ.* **1991**, *37*, 35–46. [[CrossRef](#)]
46. Yang, Y.T.; Yang, C.Y. Detection of seagrass distribution changes from 1991 to 2006 in Xincun Bay, Hainan, with satellite remote sensing. *Sensors* **2009**, *9*, 830–844. [[CrossRef](#)]
47. L Heidi, M.D.; Richard, C.Z. Ocean color remote sensing of seagrass and bathymetry in the Bahamas Banks by high-resolution airborne imager. *Limnol. Oceanogr.* **2003**, *48*, 444–455.
48. Aljenaid, S.; Ghoneim, E.; Abido, M.; AlWedhai, K.; Khadim, G.; Mansoor, S.; Mohd, W.E.D.; Hameed, N.A. Integrating remote sensing and field survey to map shallow water benthic habitat for the Kingdom of Bahrain. *J. Environ. Sci. Eng.* **2017**, *B6*, 176–200. [[CrossRef](#)]
49. Thach, N.N. *The Principles of Remote Sensing, Geographic Information Systems and Global Positioning Systems*; Ha Noi National University; University of Natural Sciences: Ha Noi, Vietnam, 2011.
50. Sánchez, C.N.; Rodríguez, P.D.; Couñago, E.; Aceña, S.; Freire, J. Using vertical Sidescan Sonar as a tool for seagrass cartography. *Estuar. Coast. Shelf Sci.* **2012**, *115*, 334–344. [[CrossRef](#)]
51. Braun, A.; Hochschild, V. Potential and Limitations of Radar Remote Sensing for Humanitarian Operations. *J. Geogr. Inf. Sci.* **2017**, *1*, 228–243. [[CrossRef](#)]
52. Komatsu, T.; Igarashi, C.; Tatsukawa, K.I.; Nakaoka, M.; Hiraishi, T.; Taira, A. Mapping of seagrass and seaweed beds using hydro-acoustic methods. *Fish. Sci.* **2002**, *68*, 580–583. [[CrossRef](#)]
53. May-Lin, B.Y.; Ching-Lee, W. Seasonal growth rate of Sargassum species at Teluk Kemang, Port Dickson, Malaysia. *J. Appl. Phycol.* **2013**, *25*, 805–814. [[CrossRef](#)]
54. Pham, H.T.; Nguyen, H.D.; Nguyen, X.H.; Nguyen, T.L. Study on the variation of seagrass population in coastal waters of Khanh Hoa province, Vietnam. *Coast. Mar. Sci.* **2006**, *30*, 167–173.
55. Ha, N.T.; Manley, H.M.; Pham, T.D.; Hawes, I. A Comparative Assessment of Ensemble-Based Machine Learning and Maximum Likelihood Methods for Mapping Seagrass Using Sentinel-2 Imagery in Tauranga Harbor, New Zealand. *Remote Sens.* **2020**, *12*, 355. [[CrossRef](#)]
56. Ha, N.T.; Kunihiro, Y.; Son, H.P.T. Seagrass mapping using ALOS AVNIR-2 data in Lap An Lagoon, Thua Thien Hue, Viet Nam. In Proceedings of the SPIE—The International Society for Optical Engineering, Washington, DC, USA, 21 November 2012.

57. Pham, T.D.; Xia, J.; Ha, N.T.; Bui, D.T.; Le, N.N.; Tekeuchi, W. A Review of Remote Sensing Approaches for Monitoring Blue Carbon Ecosystems: Mangroves, Seagrasses and Salt Marshes during 2010–2018. *Sensors* **2019**, *19*, 1933. [[CrossRef](#)]
58. The Prime Minister of Vietnam. *Decision No. 61/QĐ-TTg, the Socio Economic Development of Central Coast Vietnam Up to 2020 (Vietnamese)*; The Prime Minister: Ha Noi, Vietnam, 2008.



© 2020 by the authors. Licensee MDPI, Basel, Switzerland. This article is an open access article distributed under the terms and conditions of the Creative Commons Attribution (CC BY) license (<http://creativecommons.org/licenses/by/4.0/>).